IEEE Access
Multidisciplinary | Rapid Review | Open Access Journal

Received February 17, 2021, accepted March 5, 2021, date of publication March 12, 2021, date of current version March 22, 2021.

Digital Object Identifier 10.1109/ACCESS.2021.3065738

Comparative Study of Electromagnetic Performance of Stator Slot PM Machines

H. QU AND Z. Q. ZHU, (Fellow, IEEE)
Department of Electronic and Electrical Engineering, The University of Sheffield, Sheffield S1 3JD, U.K.
Corresponding author: Z. Q. Zhu (z.q.zhu@sheffield.ac.uk)

ABSTRACT This paper firstly explains how the stator slot PM (SSPM) machines have evolved from the conventional flux reversal PM machines (FRPMs), by placing the magnets over the tooth tips or between the tooth tips. The influence of tooth tips and PM configurations of five types of SSPM machines with various PM structures in stator slots, two with tooth tips and three without tooth tips, on the electromagnetic performance are then investigated and compared. It shows that, no matter what winding configurations (non-overlapping windings or overlapping windings), appropriate design of tooth tips can increase the average torque, the SSPM machines having flux focusing structures (i.e. Halbach array PM and spoke array PM) exhibit higher torque than those without flux focusing, and the SSPM machines with tooth tips have higher PM utilization rate than those without tooth tips. Non-overlapping windings can help provide higher torque density when the prototype machine length is less than around 125mm while overlapping windings are more advantageous if the machine length is over 125mm.

INDEX TERMS Consequent pole, non-overlapping, overlapping, permanent magnet (PM), stator PM.

I. INTRODUCTION

Stator permanent magnet (PM) machines may be superior to rotor-PM machines due to a robust salient pole rotor structure as well as easy thermal management for the PMs if the forced liquid cooling is employed.

Stator PM machines can be further defined according to PM positions. Doubly salient PM (DSPM) machines have circumferentially magnetized PMs in the stator yoke [1]–[3]. The PMs are separated by the interval of the number of stator teeth equal to the phase number. DSPM machines have good PM utilization rate (defined as torque per PM volume), albeit with relatively low torque density. Switched flux PM (SFPM) machines accommodate circumferentially magnetized PMs between the stator teeth [4]–[7]. The flux focusing effect in SFPM machines enhances the torque capability significantly but deteriorates the overload capability. Flux reversal PM (FRPM) machines have a pair of PMs mounted on the stator tooth surface [8]–[10]. Despite having no flux focusing capability and relying on PM remanence and thickness, the PM arrangements and number in FRPM machines are found to have a significant impact on the torque characteristics.

The associate editor coordinating the review of this manuscript and approving it for publication was Jinquan Xu.

Stator slot PM (SSPM) machines are also among the stator PM machines and have been attracting widespread interest recently. SSPM machines can be evolved from the conventional FRPM machines, as shown in Fig. 1. Fig. 1(a) shows the schematic diagram of conventional FRPM machines [11]–[13], which has an NS-SN magnet arrangement. [14], [15] show that employing an NS-NS magnet arrangement, Fig. 1(b), can help to enhance the torque density. [16] reports that shifting the PM position by half of the PM width, Fig. 1(c), can improve the torque slightly. However, this torque improvement will be considerable when the PM shifting is employed in consequent pole FRPM (CFRPM), as shown in Fig. 1(d).

Fig. 1(d) is a type of SSPM machine and has no flux focusing capability. In [17], [18], Halbach array PM and spoke array PM are employed. The torque density is significantly improved due to the flux focusing effect. It is worth noting that the machines with PMs placed in the stator slots can be regarded as an SSPM machine, regardless of the PM magnetization direction (radially magnetized [16], [19], [20] or circumferentially magnetized [21]), PM structure (Halbach array [17] or spoke array [18]), PM arrangement or PM number [18]. In this paper, the influences of tooth tips and PM configurations of five types of SSPM machines with various PM structures in stator slots, two with tooth tips

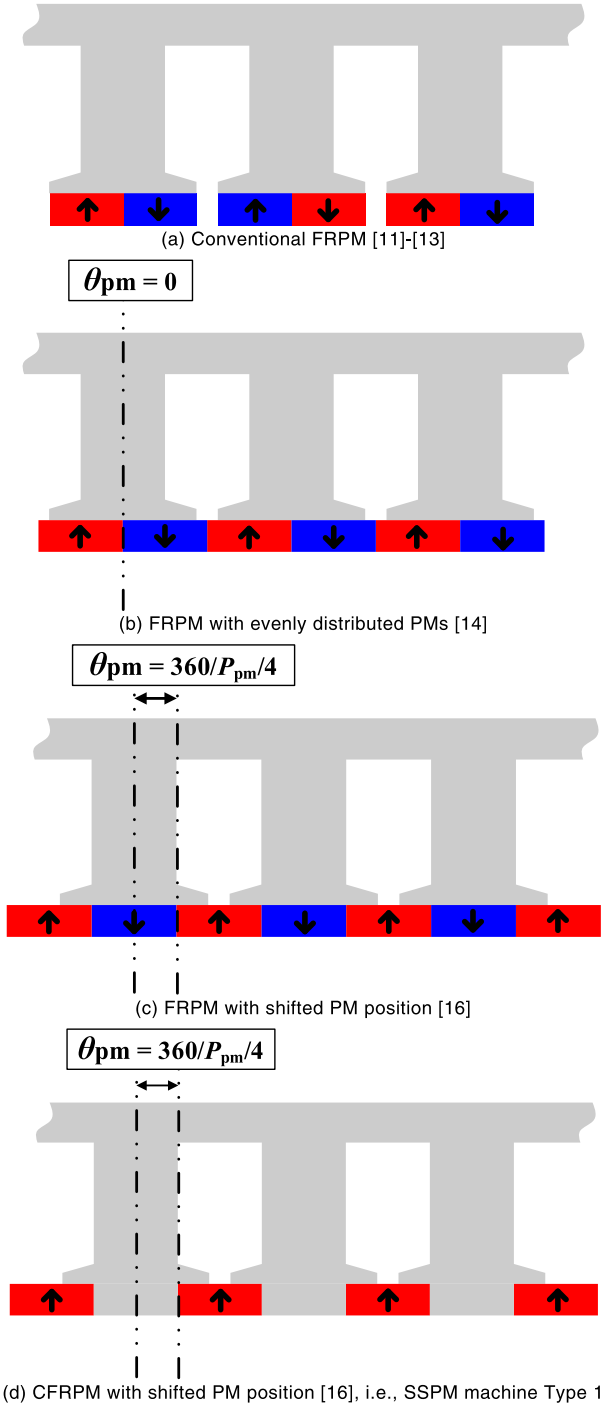

FIGURE 1. Schematic diagrams of existing FRPM/SSPM machines.

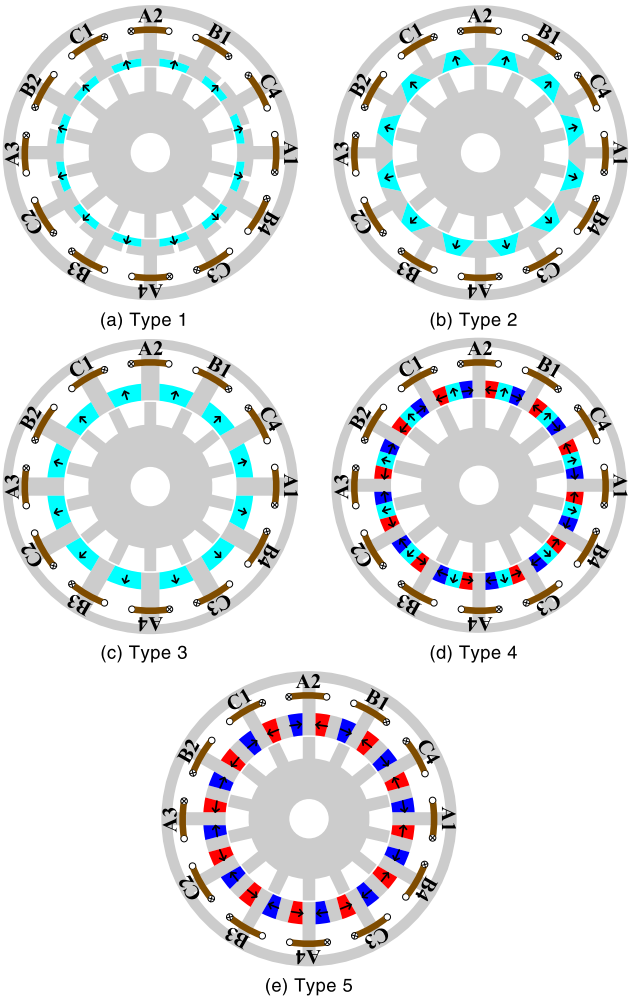

FIGURE 2. Cross sections of SSPM machines with non-overlapping windings.

and three without tooth tips, as shown in Fig. 2 (with non-overlapping windings) and Fig. 3 (with overlapping windings), respectively, on the electromagnetic performance will be investigated and compared.

This paper is arranged as follows. Firstly, the machine topologies, operation principle, slot/pole number combinations and optimal designs are introduced and analyzed in Sections II and III. The influence of tooth tip dimensions on torque characteristics is discussed in Section IV. Then, the open circuit and load electromagnetic performance of the SSPM machines with non-overlapping windings (NOW) and overlapping windings (OW) are compared in Sections V and VI, respectively. Finally, some conclusions are drawn in Section VII.

II. MACHINE TOPOLOGY AND OPERATION PRINCIPLE

In [19], [20], PMs are firstly placed in the stator slots for linear FRPM and dual PM machines, respectively. As shown in Fig. 2(a), Type 1, the PMs are placed covering the stator tooth tips and stator slot opening as well as facing the airgap. The tooth tip is determined by three parameters, d_1, th, and tp, as shown in Fig. 4(a). In Type 2, the magnets are placed between the stator tooth tips and in the stator slot opening. The tooth tip is different from the conventional one. Conventional stator tooth has a wider tooth face near the airgap to collect flux lines. However, the stator tooth in Type 2 has a narrow tooth face near the airgap to enhance the flux modulation effect. The tooth tip is determined by three parameters, d_1, d_2, and th, as shown in Fig. 4(b).

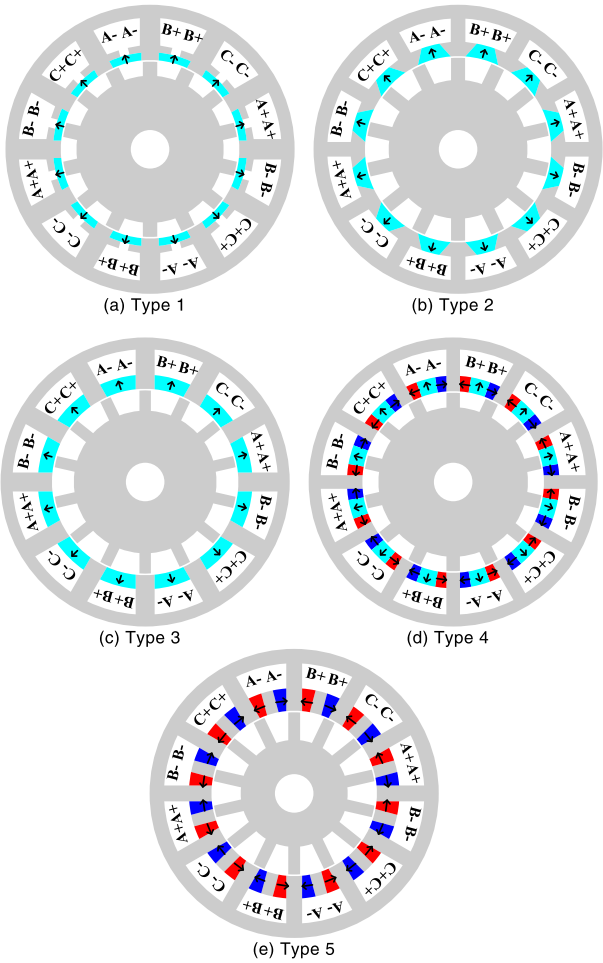

FIGURE 3. Cross sections of SSPM machines with overlapping windings.

Type 3 has no stator tooth tips. The flux lines have to pass through the air in the stator slot. Thus, the PMs in Type 3 are obviously thicker than those in Type 1. Halbach array PMs are employed in Type 4 to help to reduce the magnetic reluctance. The two side PMs are introduced to conduct and focus the flux. Compared with Type 4, Type 5 replaces the middle PMs with iron poles.

In Fig. 2, all the machines have non-overlapping windings that are wound around the stator teeth. In Fig. 3, the overlapping windings having a coil pitch of three slot pitches are employed.

The aforementioned evolution from FRPM machines to SSPM machines shows that the flux modulation effect or magnetic gearing effect is also applicable to the SSPM machines. The static PM magnetomotive force (MMF) is modulated by the rotating rotor slots and teeth, resulting in rotating MMF. Then, the rotating MMF interacts with the armature MMF, generating constant torque.

III. SLOT/POLE NUMBER COMBINATIONS AND OPTIMAL DESIGNS

Based on the flux modulation effect or magnetic gearing effect, the slot/pole number combination of the SSPM

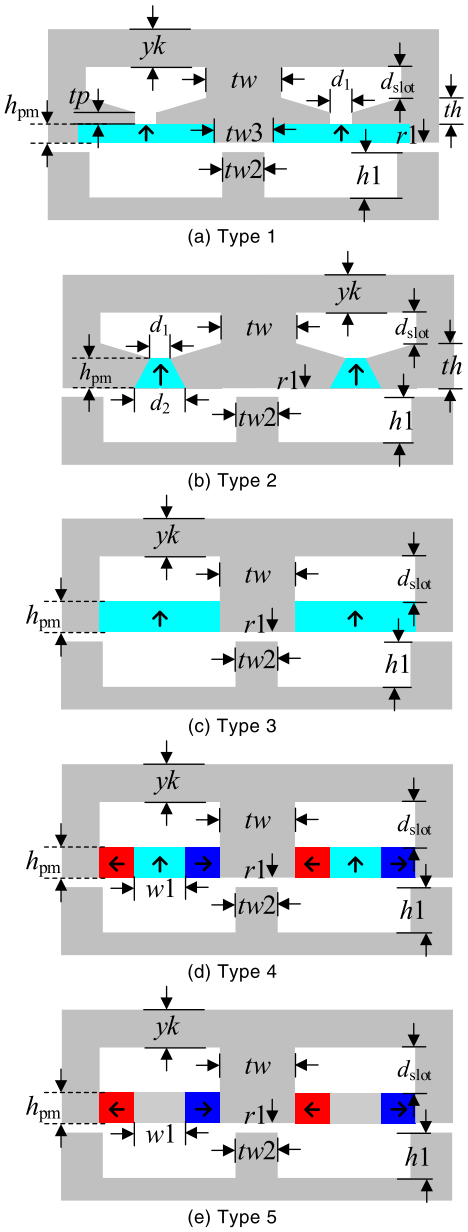

FIGURE 4. Schematic diagrams and parameters.

machines should satisfy the following equation.

$$P_a = |iP_{PM} - N_r| \tag{1}$$

where P_{PM} is the PM pole pair number, P_a is the armature winding pole pair number, N_r is the rotor pole number, i is an integer.

Fig. 5 shows the winding layouts and back EMF phasors of Type 1 with NOW and OW, and the other four types of SSPM machines have the same winding layouts. To consider the phase shift of back EMF phasors, the phasors of even-number with revised polarity are indicated with an (').

The winding factor k_w can be expressed as

$$k_w = k_d k_p \tag{2}$$

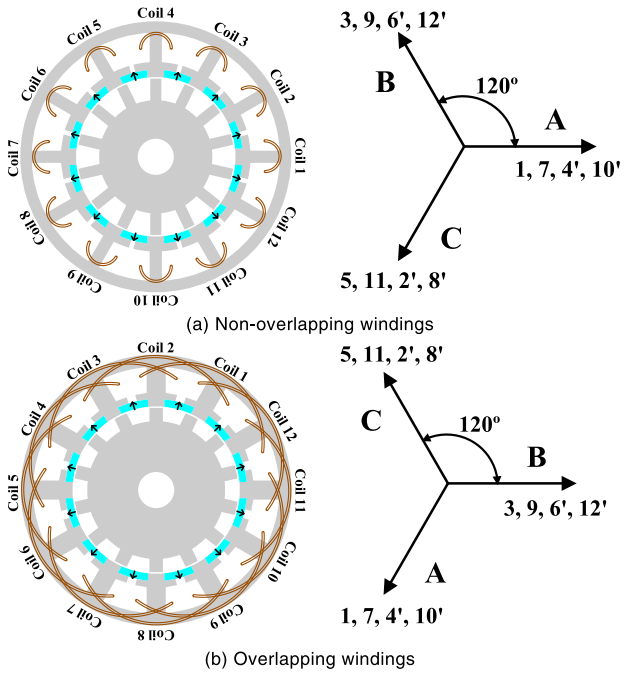

FIGURE 5. Winding layouts and back EMF phasors of type 1.

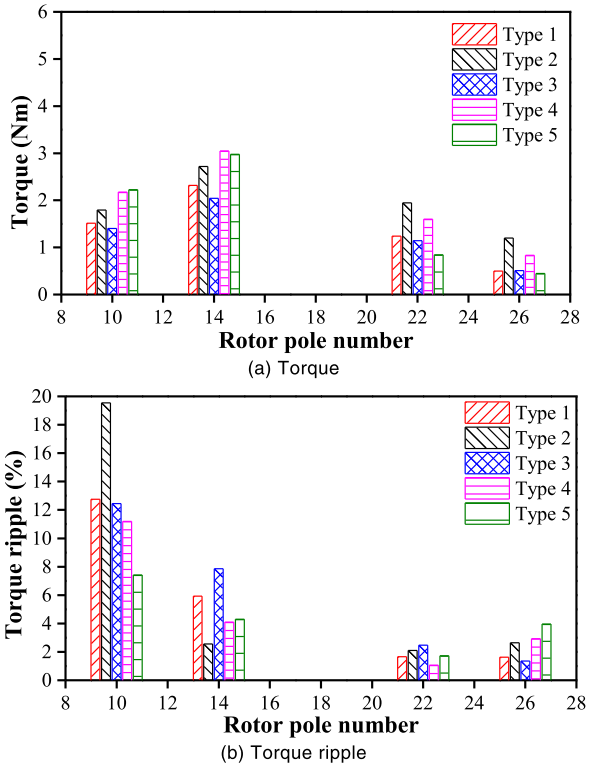

FIGURE 6. Influence of rotor pole number on torque and torque ripple when $P_a = 2$ for SSPM machines with 12 stator slots and non-overlapping windings.

where k_d is the winding distribution factor, and k_p is the pitch factor. k_d is given by

$$k_d = \frac{\sin(Q v\alpha/2)}{Q\sin(v\alpha/2)} \tag{3}$$

where Q is the number of coil-EMF phasors per phase, α is the angle between two adjacent coil-EMF phasors, and v is the harmonic order.

$$k_p = \sin(\frac{y}{y_{max}}\frac{\pi}{2}) \tag{4}$$

where y is the coil pitch and y_{max} is the coil pitch with full pitched windings.

As can be observed from Fig. 5, the winding configurations do not affect the back EMF phasors and the slot/pole number combinations. For NOW and OW, the distribution factors are the same as 1 and the pitch factors are 0.5 and 1, respectively. Hence, the winding factors of NOW and OW are 0.5 and 1, respectively.

Here, the armature pole pair number P_a is chosen as 2 (the same as in [17], [18]), to investigate the impact of tooth tips, PM configurations and winding configurations. According to (1), the rotor pole number can be selected as 10 ($i = 1$), 14 ($i = 1$), 22 ($i = 2$), and 26 ($i = 2$), etc.. Figs. 6(a) and 7(a) show that when the rotor pole number is chosen as $P_{PM} + P_a$, the highest torque can be generated. It is noted that when $N_r = 14$ and the highest torque is produced, the torque ripple is also quite low due to the combination of 12 slots 14 rotor poles (12S14R).

By comparing Figs. 6 and 7, it can be concluded that the winding configurations do not affect the optimum rotor pole number, although the specific torque values are affected. The winding configurations influence the torque performance by affecting the winding factors, magnetic saturation and flux utilization rate of flux in stator slot, which will be explained later. If saturation and flux leakage are not considered, the influence of geometric parameters can be decoupled from the winding configurations. When investigating the influence of PM thickness and tooth tips, only results with NOW will be shown since those with OW exhibit a similar tendency.

To further investigate and fairly compare the electromagnetic performance of the five types of SSPM machines, global optimizations are employed under 20W effective copper loss, with the aid of finite element software, JMAG. The geometric parameters are given in TABLEs 1 and 2.

(a) Five SSPM machines have NOW (Fig. 2) while the other five machines are with OW (Fig. 3).

(b) All the machines have the same stator outer diameter, stack length, PM material, and iron steel material.

(c) Optimized parameters, as shown in Fig. 4, are tooth tip dimensions, stator yoke/tooth widths, stator inner radius, rotor tooth width/depth, and PM thickness.

(d) The global optimizations are based on Genetic Algorithm (GA), and 30 individuals in each population with 35 generations have been employed.

(e) It should be noted that the PM volumes are not restricted, due to the fact that different SSPM machines have different PM configurations and tooth tips. For Type 5 with circumferentially PMs, the thicker the PMs are, the more

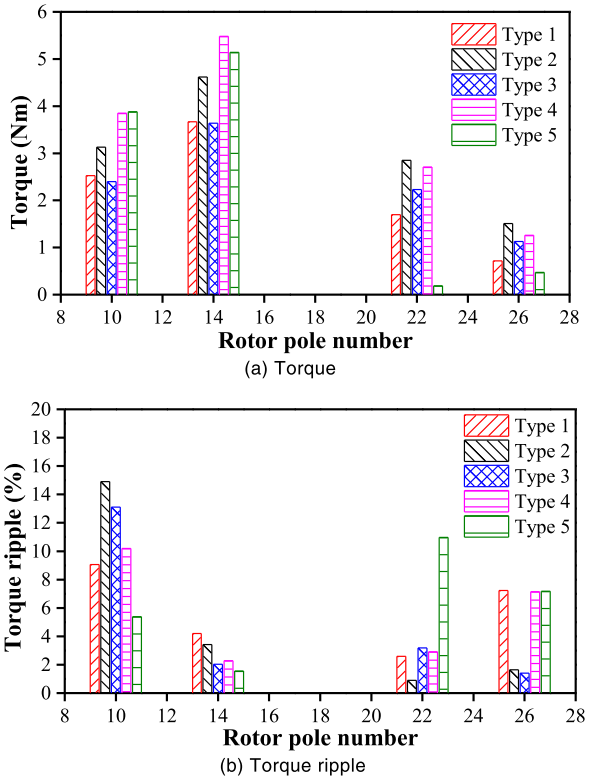

FIGURE 7. Influence of rotor pole number on torque and torque ripple when $P_a = 2$ for SSPM machines with 12 stator slots and overlapping windings.

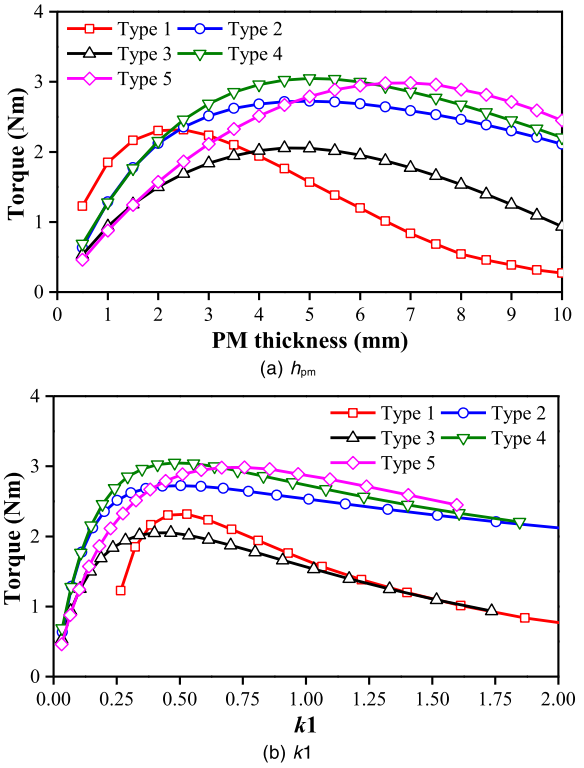

FIGURE 8. Influence of h_{pm} and $k1$ of five machines with non-overlapping windings when $P_{cu_eff} = 20$W.

TABLE 1. Parameters of optimized topologies with non-overlapping windings.

Parameter	Type 1	Type 2	Type 3	Type 4	Type 5
Stator outer diameter (mm)			90		
Stack length (mm)			25		
Airgap length (mm)			0.5		
PM volume (cm^3)	6.5	11.4	14.8	17.7	15.0
Rated speed (rpm)			600		
Armature winding pole pair number			2		
Stator yoke width (mm)	3.8	2.2	2.9	2.8	3.3
Stator inner radius (mm)	26.5	26.9	26.3	26.8	25.5
Stator tooth width (mm)	4.0	3.4	5.6	4.0	4.0
Rotor tooth width (mm)	3.7	3.8	3.6	3.9	3.8
Rotor slot depth (mm)	7.2	6.9	6.9	8.7	6.6
Number of turns per phase	104	108	104	108	104
PM thickness (mm)	2.4	5.25	5.16	5.16	6.81
Width of iron pole for Type 5 or radially magnetized PM for Type 4 (mm)	/	/	/	4.46	3.8
$tw3$ (mm)	5.5	/	/	/	/
d_1 (mm)	1.5	4.4	/	/	/
d_2 (mm)	/	10.1	/	/	/
th (mm)	2.6	5.25	/	/	/
PM material			N32EZ		
B_r, μ_r @20°C			1.13T, 1.05		
Rated voltage (V)			48		
Rated current (Arms/Apeak)			10/14.1		

TABLE 2. Parameters of optimized topologies with overlapping windings.

Parameter	Type 1	Type 2	Type 3	Type 4	Type 5
Stator outer diameter (mm)			90		
Stack length (mm)			25		
Airgap length (mm)			0.5		
PM volume (cm^3)	7.0	10.8	13.7	17.0	14
Rated speed (rpm)			600		
Armature winding pole pair number			2		
Stator yoke width (mm)	4.1	4.3	3.7	3.7	4.5
Stator inner radius (mm)	27.8	29	29	28.3	25.8
Stator tooth width (mm)	6.3	4.6	5.9	4.2	4.9
Rotor tooth width (mm)	4.5	4.4	3.6	4.2	3.7
Rotor slot depth (mm)	4.4	6.9	6.3	4.5	8.6
Number of turns per phase	92	92	92	96	92
PM thickness (mm)	2.4	4.4	4.4	4.8	7
Width of iron pole for Type 5 or radially magnetized PM for Type 4 (mm)	/	/	/	5.6	3.7
$tw3$ (mm)	5.43	/	/	/	/
d_1 (mm)	2.5	5.75	/	/	/
d_2 (mm)	/	10.55	/	/	/
th (mm)	2.1	4.4	/	/	/
PM material			N32EZ		
B_r, μ_r @20°C			1.13T, 1.05		
Rated voltage (V)			48		
Rated current (Arms/Apeak)			10/14.1		

the flux will be generated. However, for the machines with radially magnetized PMs, wider PMs can provide more PM flux. Tooth tips have a much higher magnetic permeability than air and also compete with PMs and copper for space.

The efficiency is calculated by considering the total copper loss (P_{cu_total}), iron loss (P_{iron}), PM eddy current loss

(P_{pm_eddy}), as

$$\eta = \frac{P_{em}}{P_{em} + P_{cu\_total} + P_{iron} + P_{pm\_eddy}} \quad (5)$$

where P_{em} is the output power. The total copper loss consists of the effective copper loss P_{cu_eff} and end-winding copper loss P_{cu_end}. The end-winding length per turn l_{end} is calculated as

$$l_{end} = \tau_c \pi \quad (6)$$

where τ_c is the average coil pitch of the machine.

For the distributed windings, the end winding length τ_c is calculated as

$$\tau_c = 2\pi \left(r_3 - yk - 0.5h_{slot}\right) \frac{y}{N_s} \quad (7)$$

For the concentrated windings, τ_c is calculated as

$$\tau_c = \pi \left(r_3 - yk - 0.5h_{slot}\right) / N_s + 0.5tw \quad (8)$$

in which y is the slot pitch, r_3 the stator outer radius, N_s the stator slot number, yk the stator yoke width, tw the stator tooth width, h_{slot} slot height.

The PM eddy current loss is predicted based on the material property of N32EZ (the resistivity is 1.4e-6 Ω m), and the iron loss is calculated using finite element software JMAG [22], and the iron core material is 35CS300.

To further illustrate the necessity of not restricting the PM volume, the influences of PM thickness h_{pm} and $k1$ on the average torque are investigated, as in Fig. 8. $k1$ is the ratio of $th + h_{pm}$ to the copper region depth d_{slot} (Type 1), the ratio of th to d_{slot} (Type 2) or the ratio of h_{pm} to d_{slot} (Type 3, Type 4, and Type 5). $k1$ can represent the relative ratio of magnetic loading to electrical loading. It should be noted that the PM utilization rate, i.e. the ratio of average torque per PM volume, will be discussed later in this paper.

As can be observed from Fig. 8(a), Type 1 has the smallest value of optimum PM thickness, since a thicker PM will increase the inter pole flux leakage and decrease the slot area, and hence reduce the average torque. Type 2, Type 3, and Type 4 have similar values of optimum PM thickness to maximize the average torque. These three machines need a thicker PM to produce higher PM MMF. For Type 4, a thicker PM also means more PM flux since it has two circumferentially magnetized side PMs. For Type 5 that relies on circumferentially magnetized PMs to produce flux, a thicker PM is more favorable. As can be seen, this machine has the largest value of optimum PM thickness.

From Fig. 8(b), the optimal value of $k1$ of Type 5 (with circumferentially magnetized PMs) is around 0.7 while those of the other four SSPM machines (with radially magnetized and Halbach array PMs) are around 0.5. This is when the balance is obtained between the electrical loading and the magnetic loading.

It is also worth noting that the value of $th + h_{pm}$ in Type 1 is close to that of h_{pm} in Type 3, as listed in TABLE 1. In Type 1, the tooth tips only play the role of conducting flux and have little effect on the flux modulation effect.

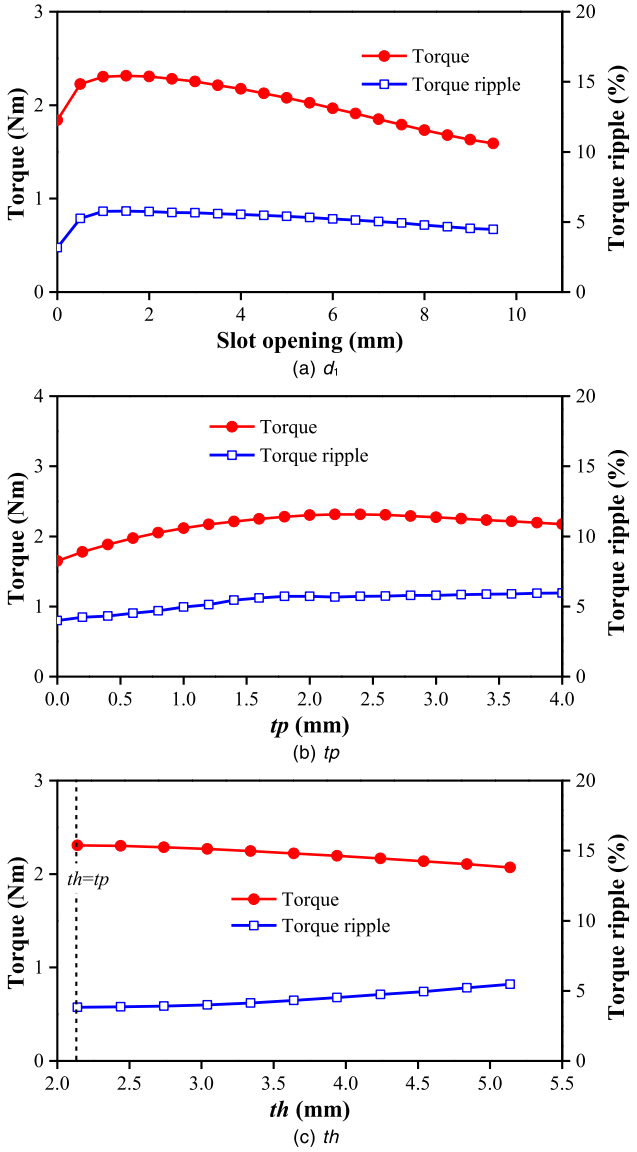

FIGURE 9. Influence of tooth tip in type 1 with non-overlapping windings on torque characteristics when P_{cu_eff} = 20W.

IV. INFLUENCE OF TOOTH TIP DIMENSIONS

The tooth tip in Type 1 helps to conduct the flux. The tooth tip dimensions mainly affect the magnetic reluctance. Fig. 9 shows the influence of the tooth tip on average torque and torque ripple under the same slot fill factor of 0.5 and the same effective copper loss of 20W. There exist optimum values of d_1 and tp to maximize the output torque. However, the torque decreases with the increase of th due to the reduced slot area. The torque ripples remain at a low level due to the 12S14R combination.

The tooth tip in Type 2 balances modulation effect and magnetic saturation. Fig. 10 shows that d_2 has greater influence on the average torque and torque ripple than d_1. When d_2 is small, the modulation effect is weak and the output torque is low. However, if d_2 is larger than 12mm, the flux path is more saturated and the output torque is reduced. Meanwhile,

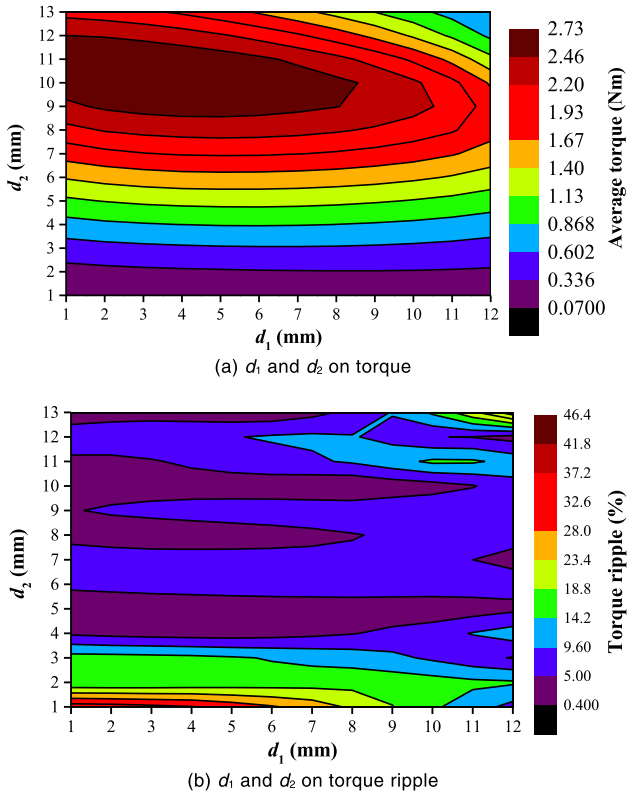

FIGURE 10. Influence of tooth tip dimensions d_1 and d_2 in type 2 with non-overlapping windings on torque characteristics when P_{cu_eff} = 20W.

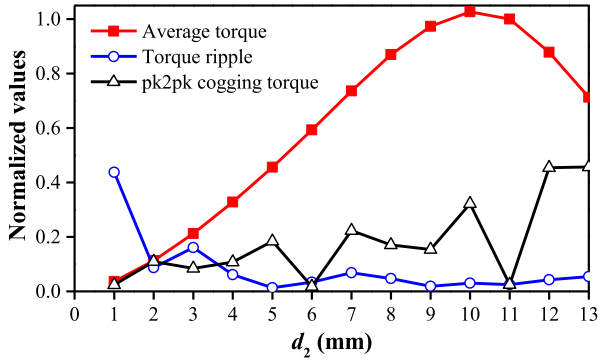

FIGURE 11. Influence of tooth tip dimension d_2 in type 2 with non-overlapping windings on torque characteristics when d_1 = 4mm.

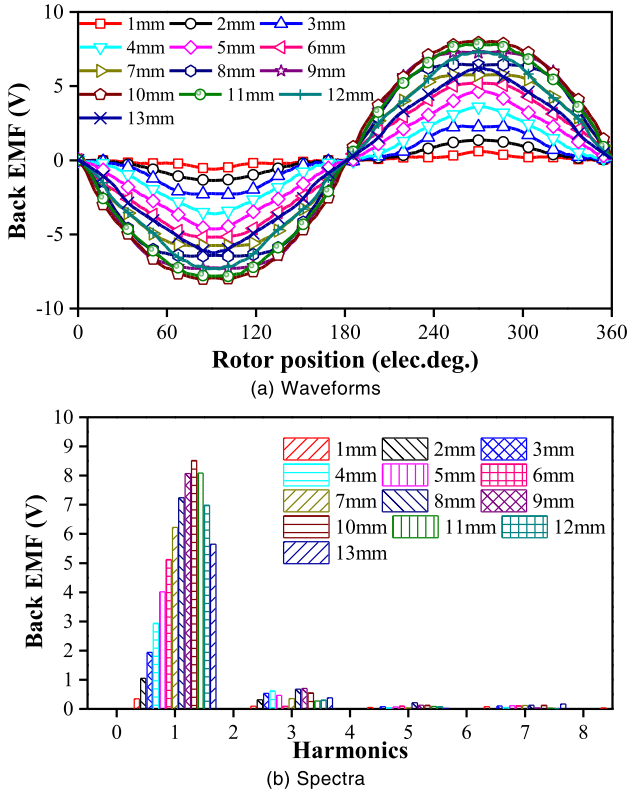

FIGURE 12. Influence of tooth tip dimension d_2 on back EMFs when d_1 = 4mm at 600rpm.

d_1 should be selected smaller than 8mm to maximize the torque. Small value of d_2 results in low average torque and high torque ripple.

When d_1 = 4mm, the influence of d_2 on the average torque, torque ripple, cogging torque (on open circuit), and back EMF (on open circuit) is illustrated in Figs. 11 and 12. The back EMF exhibits similar tendency with the average torque, since the reluctance torque is negligible, as will be shown later. Generally, the cogging torque increases with d_2, due to the increase of PM width and airgap flux density. However, two minimum points appear when d_2 is 6mm and 11mm. This is due to the effect of the change rate of magnetic permeability. It should also be noted that the torque ripple is affected by on-load cogging torque, and on-load back EMF harmonics as well as magnetic saturation. Thus, it is hard to accurately predict the on-load torque ripple based on the open circuit cogging torque and back EMF.

Fig. 13 shows that increasing *th* will reduce the output torque linearly due to the decreased copper area.

V. COMPARISON OF ELECTROMAGNETIC PERFORMANCE OF STATOR SLOT PM MACHINES WITH NON-OVERLAPPING WINDINGS

A. COMPARISON OF COGGING TORQUES

Cogging torque results from the interaction of PM MMF harmonics and airgap permeance harmonics. For the SSPM machines, the PM configurations affect the PM MMF harmonics while the stator/rotor tooth structures influence the airgap permeance. To identify the influence of tooth tips in Type 1 and Type 2 and PM structures in the other three machines, some geometric parameters, i.e. stator tooth/yoke widths, PM thickness (for Type 1, *th* is kept the same as the PM thickness in the other four machines), copper area, rotor tooth width, and rotor slot depth, are kept the same as the average values, as shown in TABLE 3. Besides, *tw*3 in Type 1 is the same as *tw* and d_2 in Type 2 is also adjusted to keep the tooth face width the same as *tw*.

Fig. 14 compares the cogging torques of the five SSPM machines. Overall, the machines exhibit very low cogging torques due to the 12 slots and 14 poles combination.

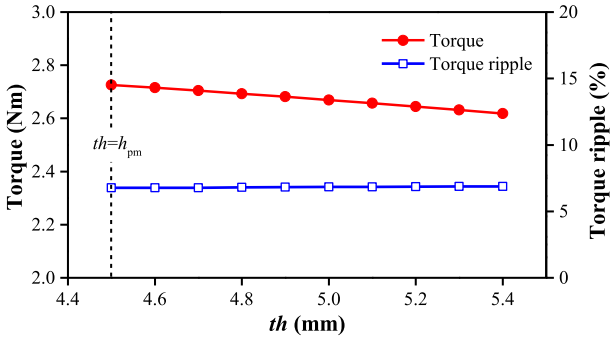

FIGURE 13. Influence of tooth tip dimension *th* in type 2 with non-overlapping windings on average torque characteristics when P_{cu_eff} = 20W.

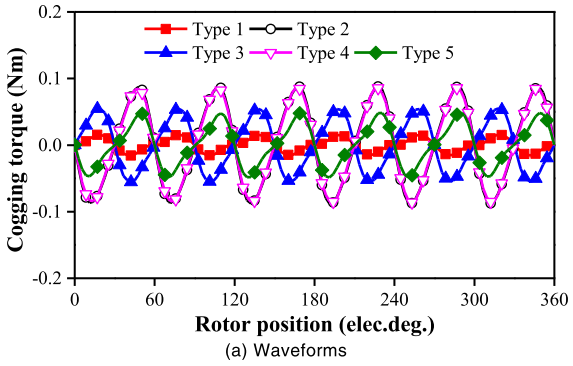

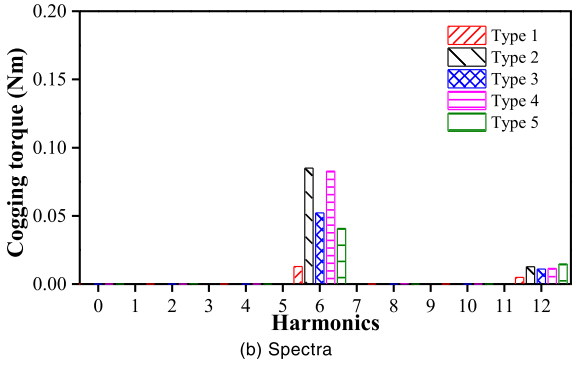

FIGURE 14. Comparison of cogging torques on open circuit.

Type 1 shows lower cogging torque than Type 3, although they have similar airgap flux density, as shown in Fig. 15. This is because the tooth tips in Type 1 reduces the change rate of the airgap permeance. Due to higher air flux density (Fig. 15) and less saturation in the stator teeth (Fig. 16), the cogging torque of Type 2 is higher than that of Type 3.

Due to higher airgap flux density Type 4 shows higher cogging torque amplitude than Type 3. Type 5 has lower cogging torque than Type 4 since the iron poles that replaces the radially magnetized PMs increases the harmonic order of the airgap permeance.

B. COMPARISON OF OTHER ELECTROMAGNETIC PERFORMANCE

In this section, the five SSPM machines with NOW are compared based on optimal designs, in terms of electromagnetic performance on open circuit and load.

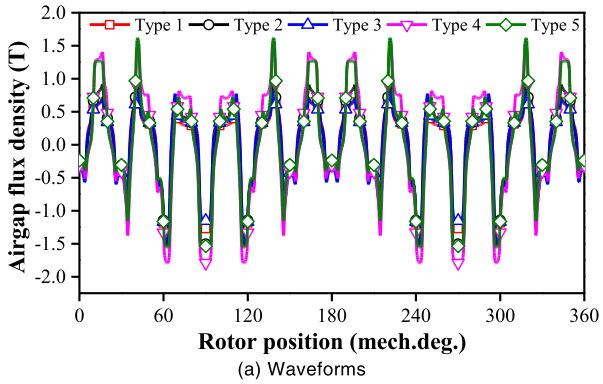

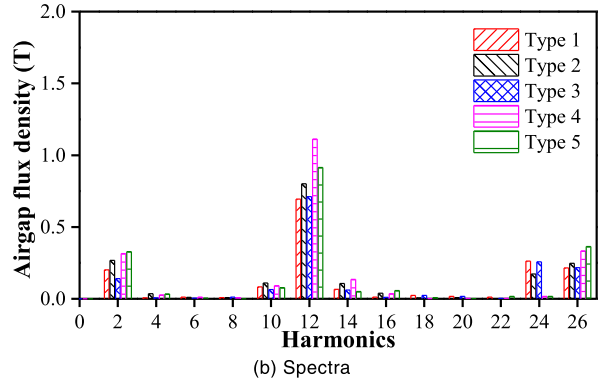

FIGURE 15. Comparison of airgap flux densities on open circuit.

TABLE 3. Parameters of topologies with non-overlapping windings.

Parameter	Type 1	Type 2	Type 3	Type 4	Type 5
Stator yoke width (mm)			3.00		
Stator inner radius (mm)			26.4		
Stator tooth width (mm)			4.2		
Rotor tooth width (mm)			3.8		
Rotor slot depth (mm)			7.3		
Number of turns per phase			106		
PM thickness (mm)	2.4	5.5			
Width of iron pole for Type 5 or radially magnetized PM for Type 4 (mm)	/	/	/	4.13	4.13
$tw3$ (mm)	4.2	/	/	/	/
d_1 (mm)	1.5	4.4	/	/	/
d_2 (mm)	/	9.55	/	/	/
th (mm)	3.1	5.5	/	/	/

In Fig. 17, the flux density distributions on open circuit of the five machines are shown. Fig. 18 compares the airgap flux densities of the five machines when the rotors are slotless, which indicates the strength of PM MMF. The PM pole pair number is N_s and hence the PM MMF harmonics are nN_s^{th}. The 12^{th} harmonic is the most dominant. Fig. 18(b) shows that Type 5 shows the highest 12^{th} harmonic and Type 4 has the second highest. Type 4 and Type 5 can focus the flux and thus exhibit higher 12^{th} PM MMF harmonic than the value of remanent flux density. In contrast, Type 1, Type 2 and Type 3 show weaker PM MMF. Type 2 can produce higher PM MMF than Type 1 due to higher PM thickness. Type 3 exhibits lower PM MMF than Type 1 due to the larger magnetic reluctance.

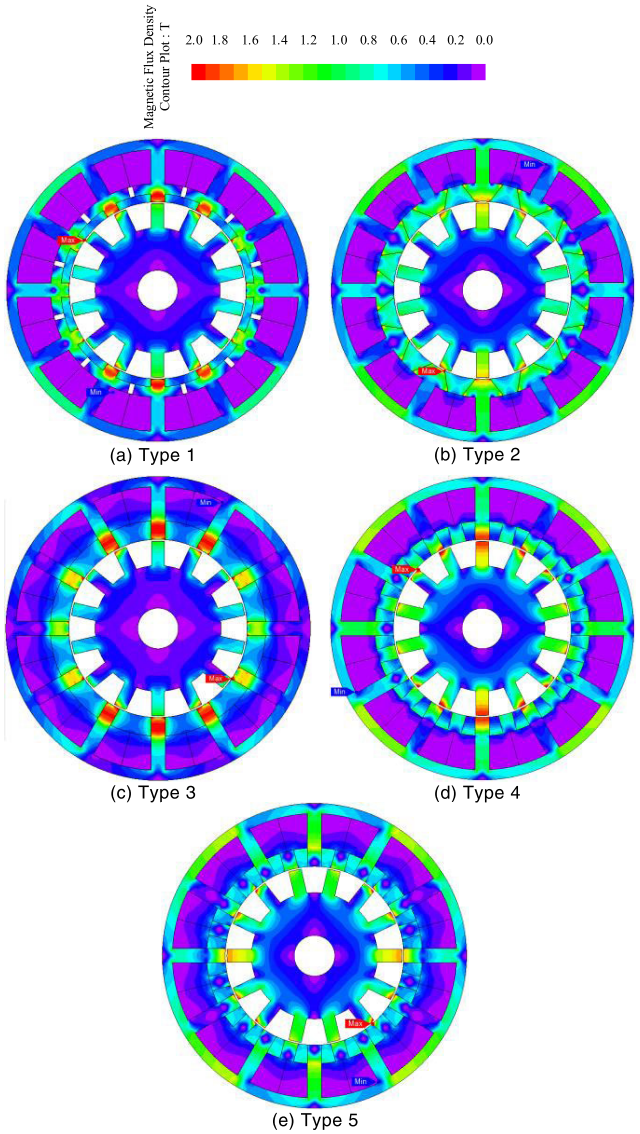

FIGURE 16. Comparison of flux density distributions on open circuit.

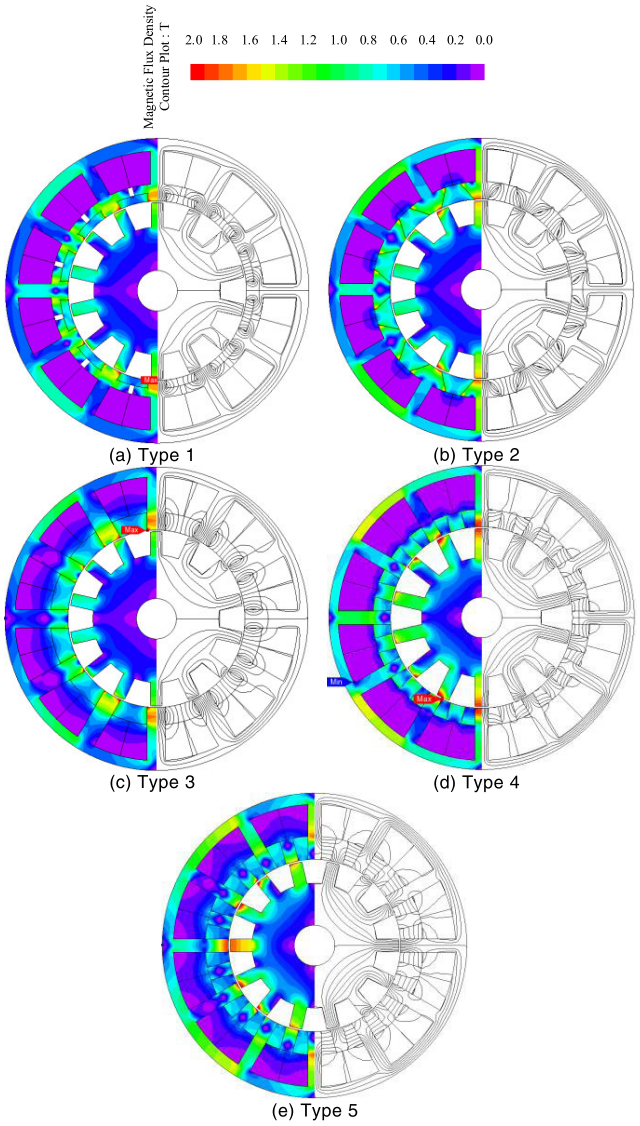

FIGURE 17. Comparison of flux density distributions on open circuit.

In Fig. 19, the back EMFs on open circuit at 600rpm are compared. As can be observed, Type 4 and Type 5 show the highest back EMF while Type 3 exhibits the lowest. This can be expected from Fig. 18(b) in which Type 4 and Type 5 have the highest 12th airgap flux density component while Type 3 exhibits the lowest 12th airgap flux density component.

Fig. 20 compares the electromagnetic torques of the five machines. Type 4 delivers the highest torque although it shows the second highest back EMF. This is due to the better overload capability of Type 4 than Type 5, as shown in Fig. 21(b). By comparing Type 1 and Type 3, it can be concluded that tooth tip can help to improve the torque density, despite the fact that Type 3 consumes a much higher PM volume. When the PMs are placed between the tooth tips, as in Type 2, appropriate design of the tooth tip can help the machine to produce 33% higher torque density compared with Type 3, together with reduced PM volume.

TABLE 4. Flux weakening factors using frozen permeability method at 5000rpm.

	Type 1	Type 2	Type 3	Type 4	Type 5
I_d (A)	-9.49	-12.65	-11.54	-13.88	-13.32
I_q (A)	4.15	5.16	5.78	2.65	4.74
L_d (mH)	0.89	0.73	0.63	0.59	0.68
Ψ_{PM} (mWb)	8.39	9.91	7.75	12.13	11.58
K_{fw}	1.5	1.04	1.15	0.68	0.83

All the five machines exhibit negligible reluctance torque, as in Fig. 21(a). It can be observed that Type 4 and Type 5 have better overload capability than Type 1 and Type 3, as shown in Fig. 21 (b). The overload capability can also be indicated by the inductance, as shown in Fig. 22. Type 4 has the lowest inductance versus Q-axis current, and therefore, has the best overload capability.

Fig. 23 shows the torque and power versus the speed of the five machines calculated according to [23]. Here, a space vector PWM control strategy is employed, the DC voltage is 48V and the maximum current is 10Arms. Type 4 has higher

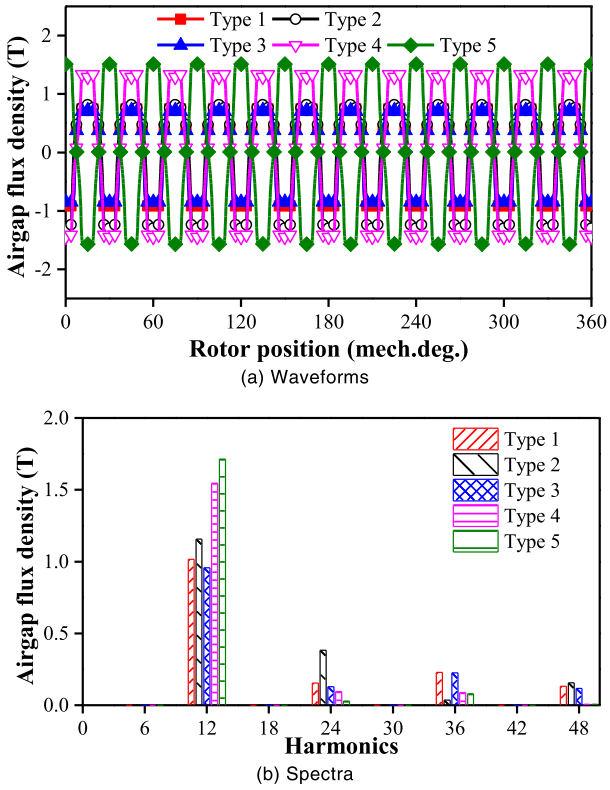

FIGURE 18. Comparison of airgap flux densities with slot-less rotors.

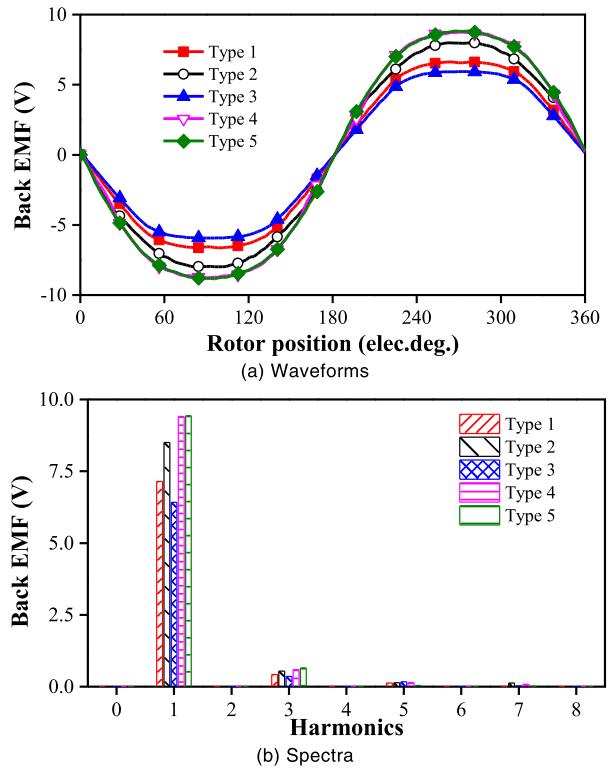

FIGURE 19. Comparison of back EMFs on open circuit at 600rpm.

corner speeds than the other four machines, due to the lowest inductances.

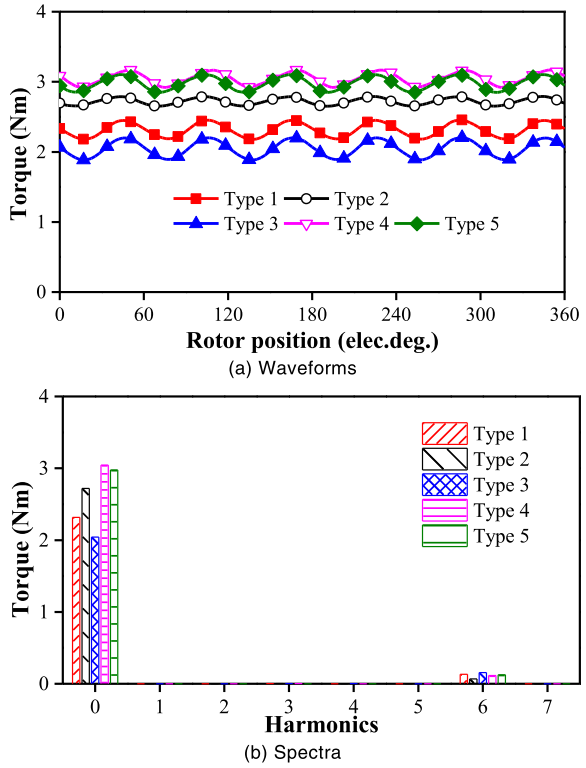

FIGURE 20. Comparison of electromagnetic torques when P_{cu_eff} = 20W.

Based on [24], a flux weakening factor K_{fw} can be defined as

$$K_{fw} = \frac{L_d I_{max}}{\psi_{PM}} \tag{9}$$

in which Ψ_{PM} is the on-load PM flux linkage, L_d is the D-axis inductance. Both Ψ_{PM} and L_d are calculated using the frozen permeability method. The load conditions are obtained from the operation points at 5000rpm on the curves of the torques versus the speed. The specific D-/Q-axis currents are listed in TABLE 4. K_{fw} can be an index for the trade-off between the torque capability in the constant torque region and the flux weakening capability in the constant power region. Ideally, K_{fw} should be as close to 1 as possible.

As listed in TABLE 4, K_{fw} of Type 1 and Type 3 is larger than 1 while that of Type 4 and Type 5 is smaller than 1. This is due to the fact that Type 4 and Type 5 have higher PM fluxes but lower D-axis inductances, compared with the other three machines. In contrast, the torque capability and flux weakening capability of Type 2 are better balanced. Type 4 and Type 5 exhibit the highest power of 567W while Type 2 shows 5% lower power of 540W.

Besides, the flux weakening factors of Type 1 and Type 3 are larger than 1 due to larger D-axis inductances. The maximum powers of Type 1 and Type 3 are 372W and 471W, respectively.

Fig. 24 shows the efficiencies versus speed while Figs. 25 and 26 illustrate the iron loss and PM eddy current loss variations. Type 4 always exhibits the highest efficiency

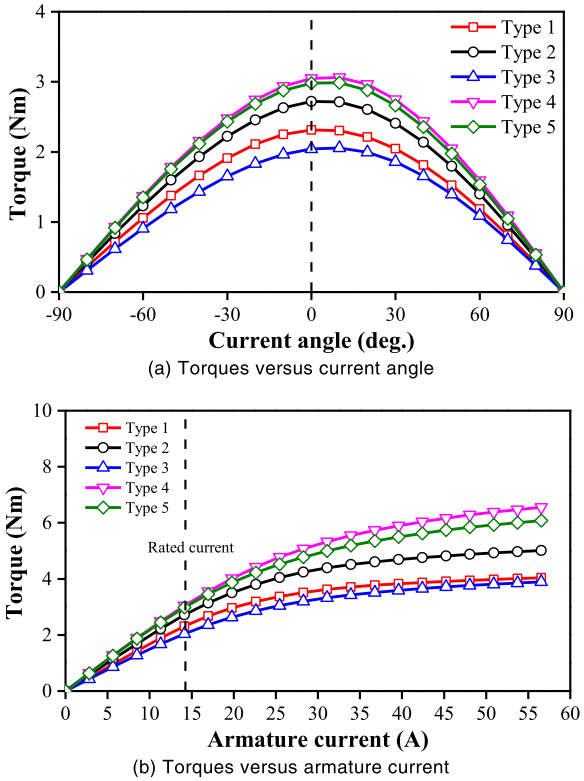

FIGURE 21. Comparison of torques versus current angle and armature current.

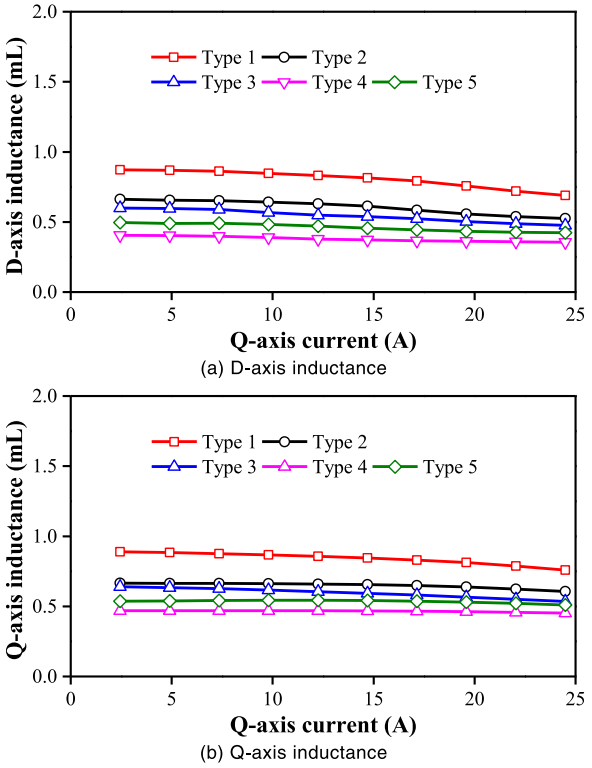

FIGURE 22. D-/Q-axis inductances versus Q-axis current.

due to its highest average torque. For Type 1 and Type 2, since the armature reactions are stronger, as can be indicated by the overload capability and inductances, they exhibit higher PM eddy current loss than the other three machines. Type 3 has the lowest airgap flux density and hence the lowest iron loss. In contrast, other four machines have similar iron losses.

It should be noted that Type 3 has lower efficiency compared with Type 1 and Type 2 when the speed is lower than 1800rpm and 4800rpm, respectively, due to the lower average torque. However, at 12000rpm, Type 3 shows the second highest efficiency thanks to the lowest flux density and weak armature reaction, and consequently the lowest iron loss and the second lowest PM eddy current loss.

VI. COMPARISON OF ELECTROMAGNETIC PERFORMANCE OF STATOR SLOT PM MACHINES WITH OVERLAPPING WINDINGS

The SSPM machines with OW exhibit similar open circuit electromagnetic performance, i.e. flux density distributions, airgap flux densities, cogging torques, with the SSPM machines with NOW. Considering the winding factor, the back EMFs are also predictable. Therefore, this section mainly focuses on the on-load electromagnetic performance and the comparison between NOW and OW.

Fig. 27 illustrates the torques of the SSPM machine with OW. Similar tendencies can be observed by comparing

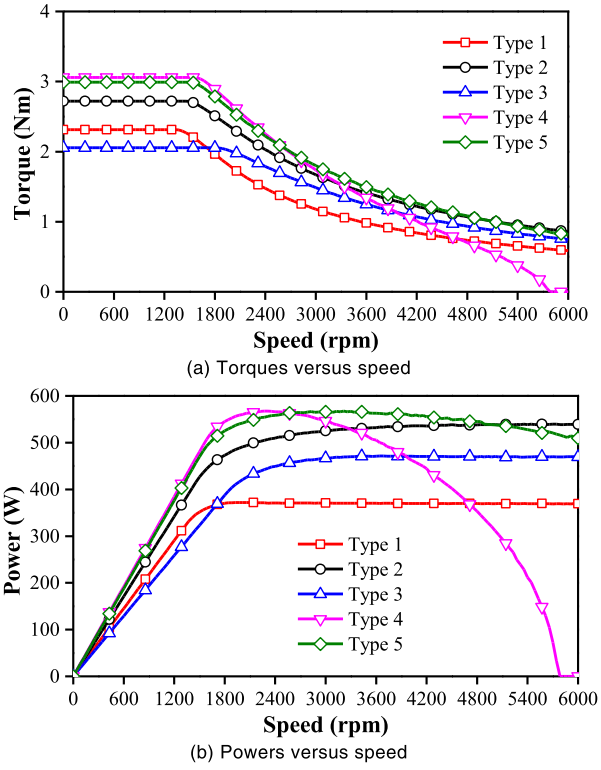

FIGURE 23. Comparison of characteristics of torque/power versus speed.

Figs. 20 and 27. The machines with Halbach array and spoke array PMs can significantly improve the torque density no matter what winding configurations.

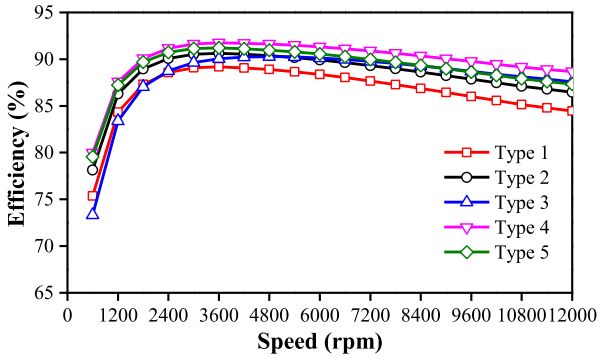

FIGURE 24. Efficiencies versus speed when $I_d = 0$ and $I_q = 14.14$A.

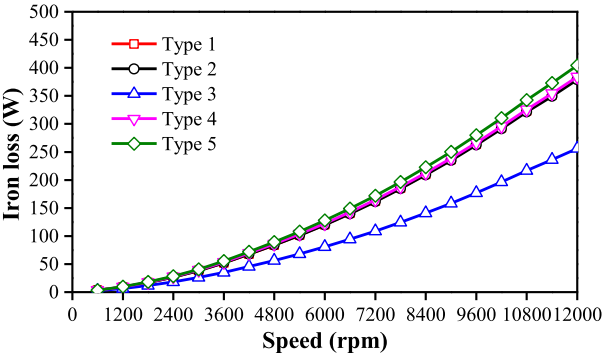

FIGURE 25. Iron losses versus speed when $I_d = 0$ and $I_q = 14.14$A.

TABLE 5. Comparison of electromagnetic performance of SSPM machines with non-overlapping windings.

	Type 1	Type 2	Type 3	Type 4	Type 5
Torque (Nm)	2.32	2.72	2.04	3.05	2.98
Torque ripple (%)	5.93	2.56	7.86	4.10	4.30
PM volume (cm^3)	6.5	11.4	14.8	17.7	15.0
Torque per PM volume (Nm/cm^3)	0.36	0.24	0.138	0.17	0.20
Power factor	0.62	0.76	0.71	0.88	0.84

TABLE 6. Comparison of electromagnetic performance of SSPM machines with overlapping windings.

	Type 1	Type 2	Type 3	Type 4	Type 5
Torque (Nm)	3.66	4.62	3.64	5.48	5.14
Torque ripple (%)	4.2	3.4	2.0	2.3	1.6
PM volume (cm^3)	7.0	10.8	13.7	17.0	14.0
Torque per PM volume (Nm/cm^3)	0.52	0.43	0.27	0.32	0.37
Power factor	0.46	0.57	0.54	0.69	0.59

TABLE 7. Flux weakening factors using frozen permeability method at 5000rpm.

	Type 1	Type 2	Type 3	Type 4	Type 5
I_d (A)	-6.38	-8.93	-8.72	-10.83	-8.73
I_q (A)	3.98	4.67	5.33	5.52	4.33
L_d (mH)	2.37	2	1.72	1.83	2.29
Ψ_{PM} (mWb)	15.76	17.33	14.28	22.36	20.62
K_{fw}	2.13	1.63	1.71	1.16	1.57

From the specific torque values listed in TABLEs 5 and 6, the torque improvements from NOW to OW are 58%, 70%, 78%, 80%, and 72%, respectively, which are smaller than the winding factor improvement of 100%. This is related to the

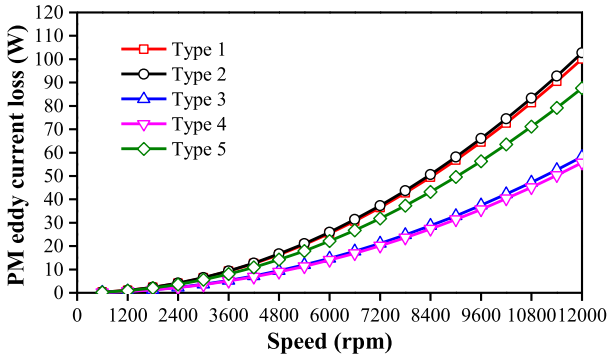

FIGURE 26. PM eddy current losses versus speed when $I_d = 0$ and $I_q = 14.14$A.

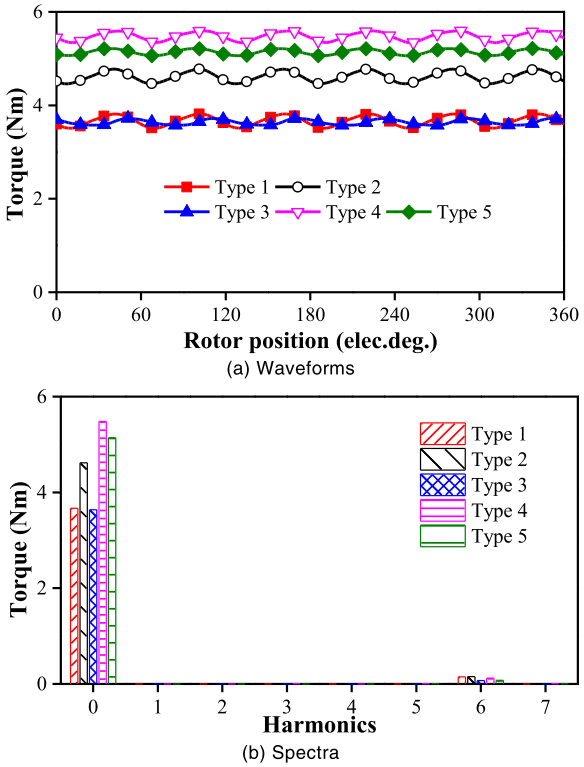

FIGURE 27. Comparison of electromagnetic torques when $P_{cu_eff} = 20$W.

magnetic saturation of the iron core, the overload capability, and the amount and the utilization rate of the flux in the stator slots (as will be illustrated later). The better the overload capability, the larger the improvement. As can be observed from Figs. 21 and 28, Type 4 has the best overload capability and hence the largest improvement.

The tooth tips in Type 1 are of significant importance in reducing the PM cost and improving the PM utilization rate. Compared with Type 3, Tooth tips in Type 2 can increase the torque by around 30%, together with 60%-74% higher torque per PM volume. The torque ripple reduction from NOW to OW results from the torque increase. It can also be observed that higher power factors are achieved by employing NOW, which is due to the shorter flux path and consequently smaller inductances, as shown in Figs. 22 and 29.

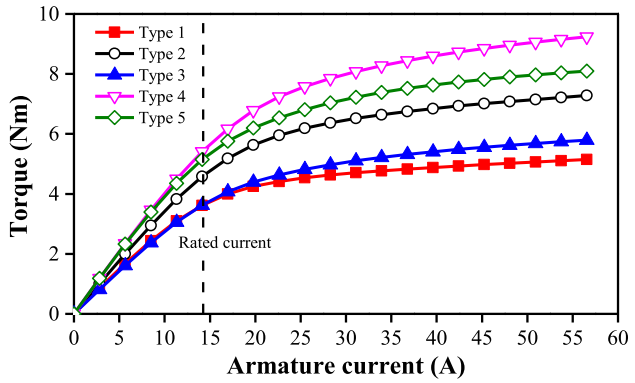

FIGURE 28. Comparison of torques versus current angle and armature current.

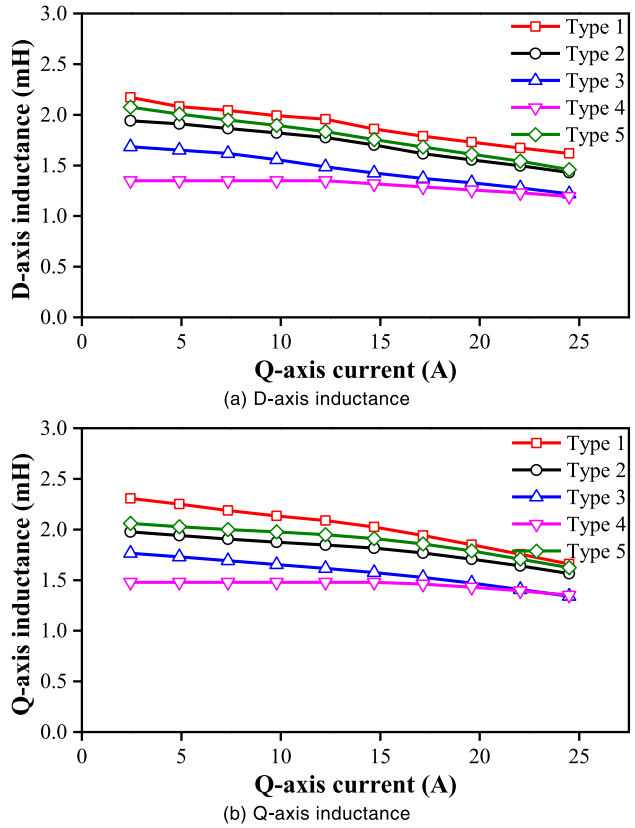

FIGURE 29. D-/Q-axis inductances versus Q-axis current.

By comparing the torque values of Type 1 and Type 3 with OW, it can be seen that although the tooth tips in Type 1 decrease the magnetic reluctance, a similar effect can be achieved at the cost of increased PM volume. However, when employing NOW, Type 1 has better torque performance. This is because that in Type 1 there is almost no flux in the stator slot, while the PM flux in Type 3 has to pass through the stator slot and OW can better utilize the flux in the stator slot since the coil span is larger.

Type 1 exhibits the highest inductances while Type 4 shows the lowest, with NOW or OW. In the SSPM machines with NOW, Type 2 has higher inductance than Type 3 and Type 5.

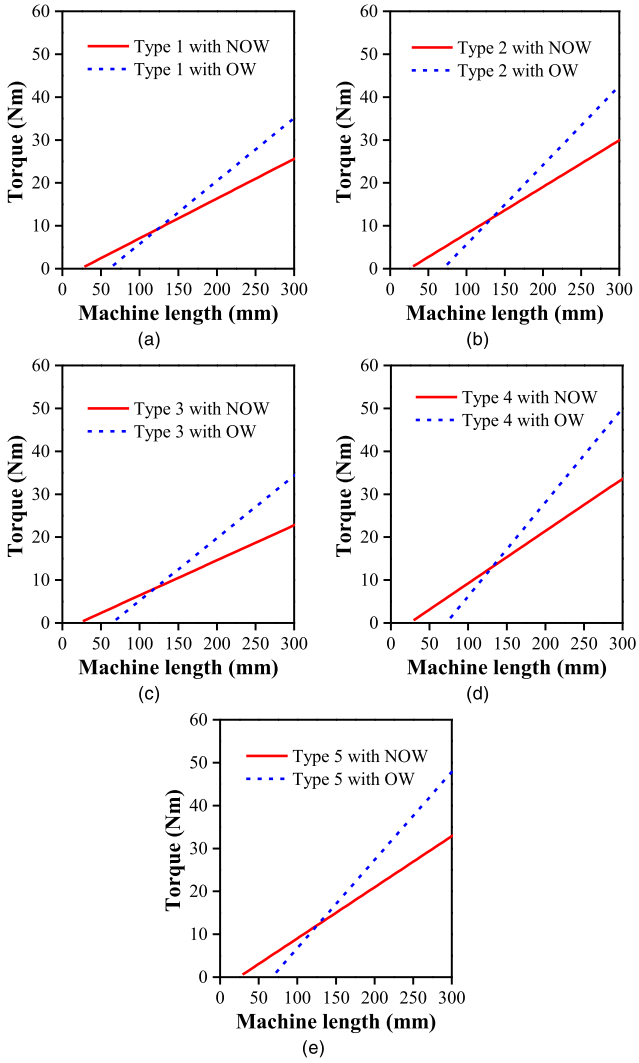

FIGURE 30. Torques versus machine length.

However, in the machines with OW, Type 5 exhibits higher values of inductances than Type 2 and Type 3. In addition to the turn number difference listed in TABLEs 1 and 2, this inconsistency between NOW and OW is because the larger coil span in OW increases the utilization rate of the flux in the stator slot. On the other hand, Type 2 has much less flux passing through the stator slot than Type 3 and Type 5, as shown in Fig. 17.

Fig. 30 compares the torque versus machine length. The machine length is $l_s + h_{end}$. h_{end} is the height of end-winding. The volume of the end-winding V_{end} and the volume of the effective winding V_{eff} satisfy (10).

$$V_{end}/V_{eff} = l_{end}/l_s \tag{10}$$

$$V_{end} = \pi(r_b^2 - r_t^2)h_{end} \tag{11}$$

$$V_{end} = S_{slot}l_s \tag{12}$$

where r_b is the radius of slot bottom, r_t is the radius of slot top, S_{slot} is the total slot area.

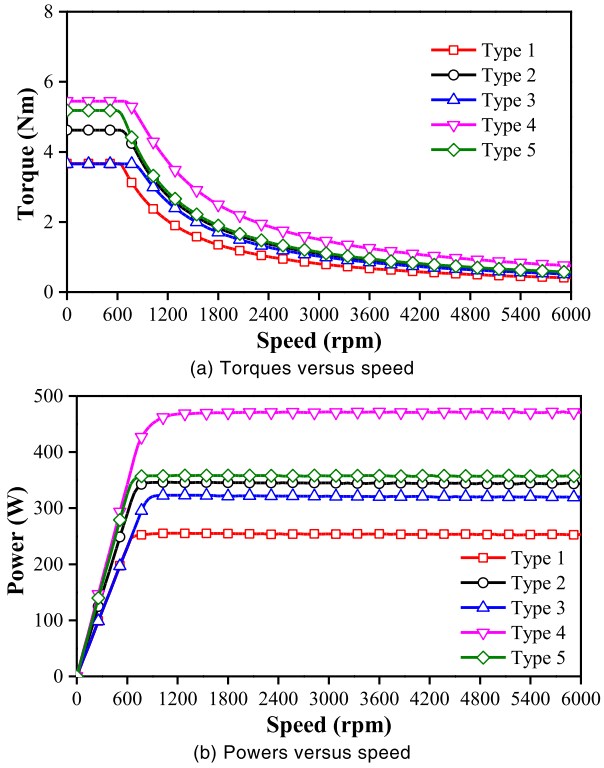

FIGURE 31. Comparison of characteristics of torque/power versus speed.

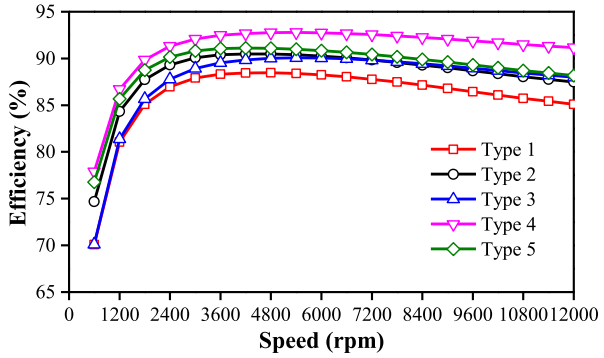

FIGURE 32. Efficiencies versus speed of machines with OW when $I_d = 0$ and $I_q = 14.14$A.

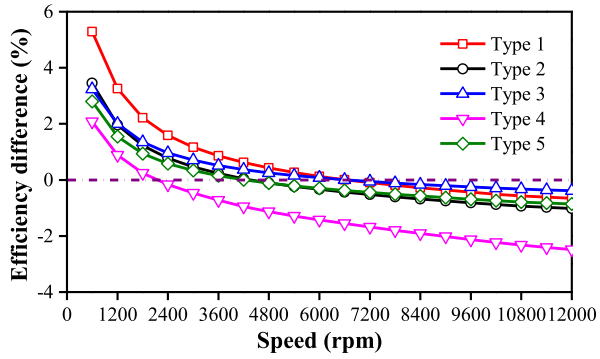

FIGURE 33. Efficiency differences between the machines with NOW and OW.

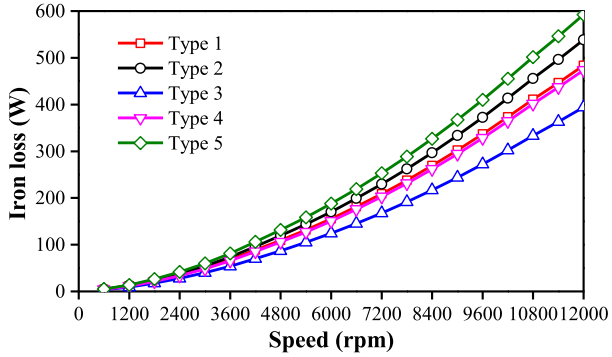

FIGURE 34. Iron losses versus speed of machines with OW when $I_d = 0$ and $I_q = 14.14$A.

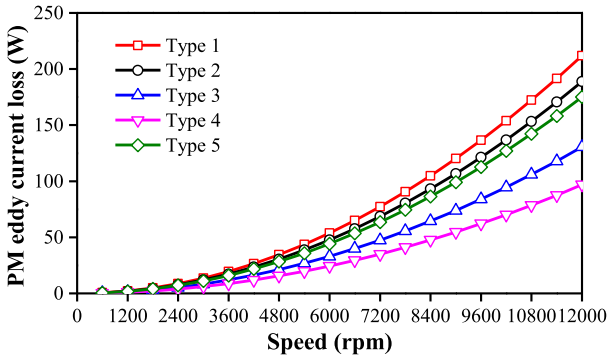

FIGURE 35. PM eddy current losses versus speed of machines with OW when $I_d = 0$ and $I_q = 14.14$A.

As can be observed, the SSPM machines with NOW are more advantageous in producing higher torques when the machine length is shorter than 125mm. However, if the machine length is longer than 125mm, OW is preferable.

Fig. 31 shows the torque and power versus speed for the machines with OW, based on the aforementioned calculation method. The corner speeds of the machines with OW are around half of those of the machines with NOW due to the influence of back EMFs and inductances. The flux weakening factors, as listed in TABLE 7, are also calculated based on the aforementioned method. As can be seen, the machines with OW have greater flux weakening factors than those with NOW, due to the fact that the increases of the PM fluxes are much higher than those of the D-axis inductances. K_{fw} of Type 4 with OW is the closest to 1, and thus showing the highest power of 470W.

Fig. 32 shows the efficiencies versus speed of the machines with OW. Similar to the machines with NOW, Type 4 exhibits the highest efficiency due to the highest torques.

Fig. 33 illustrates the efficiency differences between the machines with NOW and OW. As can be observed, when the speed is low, the machines with NOW show higher efficiency than those with OW, due to lower copper loss (shorter end-winding length), lower iron loss and lower PM loss (weaker armature reaction), as shown in Figs. 25, 26, 34 and 35. However, at high speed, the machines with OW have

higher efficiencies than those with NOW, due to higher output torques.

VII. CONCLUSION

In this paper, five types of stator slot PM machines with non-overlapping windings and overlapping windings were investigated and compared in terms of electromagnetic performance. Some conclusions can be drawn.

(a) Type 4 and Type 5 that have Halbach array PM and spoke array PM produce higher torque and power due to flux focusing, albeit with complex PM structures.

(b) Type 1 and Type 2 with tooth tips have higher PM utilization, and appropriate design of tooth tips can also enhance the torque density.

(c) The machines with non-overlapping windings have higher torque density and higher efficiency when the machine length is less than 125mm for the specific prototype machines and the operation speed is low, respectively, compared with those with overlapping windings.

(d) The machines with overlapping windings are more advantageous in providing higher torque and higher efficiency if the machine length is over 125mm for the specific prototype machines and the operation speed is high, respectively.

REFERENCES

[1] Z. Zhang, Y. Tao, and Y. Yan, "Investigation of a new topology of hybrid excitation doubly salient brushless DC generator," *IEEE Trans. Ind. Electron.*, vol. 59, no. 6, pp. 2550–2556, Jun. 2012.
[2] M. Cheng, K. T. Chau, and C. C. Chan, "Static characteristics of a new doubly salient permanent magnet motor," *IEEE Trans. Energy Convers.*, vol. 16, no. 1, pp. 20–25, Mar. 2001.
[3] K. T. Chau, Q. Sun, Y. Fan, and M. Cheng, "Torque ripple minimization of doubly salient permanent-magnet motors," *IEEE Trans. Energy Convers.*, vol. 20, no. 2, pp. 352–358, Jun. 2005.
[4] J. T. Chen and Z. Q. Zhu, "Winding configurations and optimal stator and rotor pole combination of flux-switching PM brushless AC machines," *IEEE Trans. Energy Convers.*, vol. 25, no. 2, pp. 293–302, Jun. 2010.
[5] W. Hua, M. Cheng, Z. Q. Zhu, and D. Howe, "Analysis and optimization of back EMF waveform of a flux-switching permanent magnet motor," *IEEE Trans. Energy Convers.*, vol. 23, no. 3, pp. 727–733, Sep. 2008.
[6] J. T. Chen, Z. Q. Zhu, S. Iwasaki, and R. Deodhar, "A novel E-core flux-switching PM brushless AC machine," in *Proc. IEEE Energy Convers. Congr. Expo. (ECCE)*, Atlanta, GA, USA, Sep. 2010, pp. 3811–3818.
[7] L. Shao, W. Hua, Z. Q. Zhu, X. Zhu, M. Cheng, and Z. Wu, "A novel flux-switching permanent magnet machine with overlapping windings," *IEEE Trans. Energy Convers.*, vol. 32, no. 1, pp. 172–183, Mar. 2017.
[8] D. S. More and B. G. Fernandes, "Analysis of flux-reversal machine based on fictitious electrical gear," *IEEE Trans. Energy Convers.*, vol. 25, no. 4, pp. 940–947, Dec. 2010.
[9] Y. Gao, R. Qu, D. Li, J. Li, and L. Wu, "Design of three-phase flux-reversal machines with fractional-slot windings," *IEEE Trans. Ind. Appl.*, vol. 52, no. 4, pp. 2856–2864, Jul. 2016.
[10] T. H. Kim and J. Lee, "A study of the design for the flux reversal machine," *IEEE Trans. Magn.*, vol. 40, no. 4, pp. 2053–2055, Jul. 2004.
[11] R. P. Deodhar, S. Andersson, I. Boldea, and T. J. E. Miller, "The flux-reversal machine: A new brushless doubly-salient permanent-magnet machine," *IEEE Trans. Ind. Appl.*, vol. 33, no. 4, pp. 925–934, Jul./Aug. 1997.
[12] C. Wang, S. A. Nasar, and I. Boldea, "Three-phase flux reversal machine (FRM)," *Proc. IEE Electr. Power Appl.*, vol. 146, no. 2, pp. 139–146, Mar. 1999.
[13] C. X. Wang, I. Boldea, and S. A. Nasar, "Characterization of three phase flux reversal machine as an automotive generator," *IEEE Trans. Energy Convers.*, vol. 16, no. 1, pp. 74–80, Mar. 2001.
[14] D. Li, Y. Gao, R. Qu, J. Li, Y. Huo, and H. Ding, "Design and analysis of a flux reversal machine with evenly distributed permanent magnets," *IEEE Trans. Ind. Appl.*, vol. 54, no. 1, pp. 172–183, Jan./Feb. 2018.
[15] H. Li and Z. Q. Zhu, "Influence of adjacent teeth magnet polarities on the performance of flux reversal permanent magnet machine," *IEEE Trans. Ind. Appl.*, vol. 55, no. 1, pp. 354–365, Jan./Feb. 2019.
[16] H. Yang, Z. Q. Zhu, H. Lin, H. Li, and S. Lyu, "Analysis of consequent-pole flux reversal permanent magnet machine with biased flux modulation theory," *IEEE Trans. Ind. Electron.*, vol. 67, no. 3, pp. 2107–2121, Mar. 2020.
[17] K. Xie, D. Li, R. Qu, Z. Yu, Y. Gao, and Y. Pan, "Analysis of a flux reversal machine with quasi-Halbach magnets in stator slot opening," *IEEE Trans. Ind. Appl.*, vol. 55, no. 2, pp. 1250–1260, Mar./Apr. 2019.
[18] H. Qu, Z. Q. Zhu, and B. Shuang, "Influences of PM number and shape of spoke array PM flux reversal machines," *IEEE Trans. Energy Convers.*, early access, Oct. 14, 2020, doi: 10.1109/TEC.2020.3031030.
[19] T. Imada and S. Shimomura, "Magnet arrangement of linear PM Vernier machine," in *Proc. Int. Conf. Electr. Mach. Syst. (ICEMS)*, Hangzhou, China, Oct. 2014, pp. 3642–3647.
[20] A. Ishizaki, T. Tanaka, K. Takasaki, and S. Nishikata, "Theory and optimum design of PM Vernier motor," in *Proc. Int. Conf. Electr. Mach. Drives*, Durham, U.K., 1995, pp. 208–212.
[21] I. A. A. Afinowi, Z. Q. Zhu, Y. Guan, J.-C. Mipo, and P. Farah, "A novel brushless AC doubly salient stator slot permanent magnet machine," *IEEE Trans. Energy Convers.*, vol. 31, no. 1, pp. 283–292, Mar. 2016.
[22] H. Sano, K. Narita, T. Asanuma, and T. Yamada, "An accurate iron loss evaluation method based on finite element analysis for permanent magnet motors," in *Proc. Int. Conf. Electr. Mach. (ICEM)*, Lausanne, Switzerland, Sep. 2016, pp. 1284–1289.
[23] G. Qi, J. T. Chen, Z. Q. Zhu, D. Howe, L. B. Zhou, and C. L. Gu, "Influence of skew and cross-coupling on flux-weakening performance of permanent-magnet brushless AC machines," *IEEE Trans. Magn.*, vol. 45, no. 5, pp. 2110–2117, May 2009.
[24] R. F. Schiferl and T. A. Lipo, "Power capability of salient pole permanent magnet synchronous motors in variable speed drive applications," *IEEE Trans. Ind. Appl.*, vol. 26, no. 1, pp. 115–123, Jan./Feb. 1990.

H. QU was born in Anhui, China, in 1987. He received the B.Eng. degree in electrical engineering from Dalian Maritime University, Dalian, China, in 2013, and the M.Sc. degree in electrical engineering from the Harbin Institute of Technology, in 2015. He is currently pursuing the Ph. D. degree with The University of Sheffield, Sheffield, U.K. From 2015 to 2017, he worked as a Research and Development Engineer with Midea. His research interests include the design of flux modulation and permanent magnet machines.

Z. Q. ZHU (Fellow, IEEE) received the B.Eng. and M.Sc. degrees from Zhejiang University, Hangzhou, China, in 1982 and 1984, respectively, and the Ph.D. degree from The University of Sheffield, Sheffield, U.K., in 1991, all in electrical engineering.

Since 1988, he has been with The University of Sheffield, where he has also been a Professor with the Department of Electronic and Electrical Engineering since 2000. He is currently the Royal Academy of Engineering/Siemens Research Chair, the Head of the Electrical Machines and Drives Research Group, the Academic Director of Sheffield Siemens Gamesa Renewable Energy Research Centre, the Director of CRRC Electric Drives Technology Research Centre, and the Director of Midea Electric Machines and Controls Research Centre. His current research interests include the design and control of permanent magnet machines and drives for applications ranging from electric vehicles through domestic appliance to renewable energy. He is also a Fellow of the Royal Academy of Engineering, U.K. He was a recipient of the 2021 IEEE Nikola Tesla Award and the 2019 IEEE IAS Outstanding Achievement Award.